Ionics (2015) 21:2227–2236
DOI 10.1007/s11581-015-1392-4

ORIGINAL PAPER

Novel nanocomposite membranes based on polybenzimidazole and Fe_2TiO_5 nanoparticles for proton exchange membrane fuel cells

Akbar Shabanikia · Mehran Javanbakht · Hossein Salar Amoli · Khadijeh Hooshyari · Morteza Enhessari

Received: 26 September 2014 / Revised: 22 December 2014 / Accepted: 15 February 2015 / Published online: 22 March 2015

Abstract In this work, Fe_2TiO_5 nanoparticles were used for improving the proton conductivity, and water and acid uptake of polybenzimidazole (PBI)-based proton exchange membranes. The nanocomposite membranes have been prepared using different amounts of Fe_2TiO_5 nanoparticles and dispersed into a PBI membrane with the solution-casting method. The prepared membranes were then physico-chemically and electrochemically characterized for use as electrolytes in high-temperature PEMFCs. The PBI/Fe_2TiO_5 membranes (PFT) showed a higher acid uptake and proton conductivity compared with the pure PBI membranes. The highest acid uptake (156 %) and proton conductivity (78 mS/cm at 180 °C) were observed for the PBI nanocomposite membranes containing 4 wt% of Fe_2TiO_5 nanoparticles (PFT_4). The PFT_4 composite membrane showed 380 mW/cm^2 power density and 760 mA/cm^2 current density in 0.5 V at 180 °C at dry condition. The above results indicated that the PFT_4 nanocomposite membranes could be utilized as proton exchange membranes for high-temperature fuel cells.

Keywords PEMFC · Polybenzimidazole · Nanocomposite · Proton exchange membrane · Proton conductivity

A. Shabanikia · M. Javanbakht (✉) · K. Hooshyari · M. Enhessari
Department of Chemistry, Amirkabir University of Technology, Tehran, Iran
e-mail: mehranjavanbakht@gmail.com

M. Javanbakht · K. Hooshyari · M. Enhessari
Fuel Cell and Solar Cell Lab, Renewable Energy Research Center, Amirkabir University of Technology, Tehran, Iran

H. S. Amoli
Faculty of Chemical Industry, Iranian Research Organization for Science and Technology, IROST, Tehran, Iran

Introduction

Proton exchange membrane (PEM) is a significant material in PEM fuel cells (PEMFC) [1]. Perfluorosulfonated polymers such as Nafion are crucial materials for the development of PEMFC [2]. However, the commercially used Nafion membrane will lose their proton conductivity due to water evaporation at elevated temperature [3]. Considerable research has been focused on commercially available polybenzimidazole (PBI) [4]. The proton conductivity value for pure PBI membrane is low and was obtained nearly 10^{-9} mS/cm. However, its proton conductivity can be enhanced by adding different inorganic acids such as phosphoric acid (PA), sulfuric acid, nitric acid, or perchloric acid. Among these acids, PA is the most extensively used due to its high boiling point, high thermal stability, and high proton conductivity even in its anhydrous form [5, 6]. The enhanced proton conductivity of PA-PBI membranes in comparison with pure PBI membranes contribute to an effective acid doping of PBI membrane and provide new proton conduction pathways. PA as an acid with excellent thermal stability and high proton conductivity is always of interest to fuel cell researchers. When the pure PBI membrane is doped with PA, PA acts as a proton conducting transporter and no water is needed for proton conduction in the membranes. The proton conductivities of PA-doped PBI (PA-PBI) membranes have been extensively investigated [7–10]. However, the mechanical properties of the PA-PBI membranes may deteriorate due to the very high PA-doping level. This has been a serious problem for the improvement of the PA-PBI membranes. Oxide-type proton conductors are very important materials for a wide range of electrochemical applications such as fuel cells or hydrogen sensors because of their promising proton conductivity at high temperatures [11]. Nanocomposite membranes are new groups of membranes

which include nanoparticles such as SiO_2, TiO_2, ZrO_2, and other compounds [12, 13].

Fe-titanates are principally found as three minerals, namely: ilmenite ($FeTiO_3$), pseudo-brookite (Fe_2TiO_5), and ulvospinel (Fe_2TiO_4). The –OH groups of Fe_2TiO_5 nanoparticles provide strong hydrogen bonding sites and increase the contents of the bound to free water into the membrane matrix. Also, nanoparticles possess a negative surface potential that are influenced by surface groups [14]. The anisotropic spin-glass behavior and photoelectrochemical and gas-sensing properties of Fe_2TiO_5 in the form of particles, thin films, or hollow spheres were studied by different groups [15–17]. The main cations in Fe_2TiO_5 nanoparticles are Ti^{4+} and Fe^{3+} [18]. According to the Lewis acid–base theory, these two cations are classified as hard acids. This means that the following polar groups will react with –OH groups of water. It seems that when Fe^{3+} cations are placed near Ti^{4+} cations in the Fe_2TiO_5 structure, it results in intensification of acidic effect and makes strong bonds with –OH groups of water. Fe_2TiO_5 single-phase nanoparticles have better hydrophilic properties in contrast with both TiO_2 and Fe_2O_3 nanoparticles [19, 20].

Lately, our group presented new PEMs based on poly(vinyl alcohol) and nanoporous silica containing phenyl sulfonic acid [21] and poly(sulfonic acid)-grafted silica nanoparticles [22] and for PEMFCs. Recently, Nafion/Fe_2TiO_5 nanocomposite membranes were prepared by dispersion of Fe_2TiO_5 nanoparticles within the commercial Nafion membranes [23]. Incorporation of Fe_2TiO_5 nanoparticles in Nafion matrix improved the thermal stability of Nafion membranes, which is important for operation of PEMFCs at elevated temperatures.

The main aim of the present work is to study the nanocomposite membranes based on PBI and crystalline orthorhombic Fe_2TiO_5 nanoparticles [24]. The membranes were physico-chemically and electrochemically characterized for use as electrolytes in PEMFCs.

Experimental

Materials

Polybenzimidazole with chemical structure of poly(2,2′-*m*-(phenylene)-5,5′-bibenzimidazole) (PBI), with a glass transition temperature of 425–435 °C and molecular weight of 59,000–62,000 g mol^{-1} was obtained from FuMa-Tech GmbH corporation. *N*,*N*-dimethylacetamide (DMAc) was purchased from Merck. Phosphoric acid (PA) was supplied by Merck. Other reagents and solvents were obtained from Sigma-Aldrich.

Synthesis of Fe_2TiO_5 nanoparticles

Fe_2TiO_5 nanoparticles were prepared according to the following procedure [24]: All of the analytical grade reagents that were used in preparation of Fe_2TiO_5 nanoparticles are iron acetyl acetonate, tetra-*n*-butyl titanate and stearic acid. Firstly, stearic acid was melted in at 73 °C. Secondly, iron acetyl acetonate was added and then dissolved to form a transparent brown solution. Thirdly, tetrabutyltitanate was added to the solution and stirred. In the fourth stage, it was cooled down at room temperature and dried in an oven to obtain dried gel. Finally, the obtained gel was calcined to obtain Fe_2TiO_5 nanoparticles in particle size range of 48 to 60 nm.

Ion exchange capacity

The ion exchange capacity (IEC) of PA-doped membranes was determined by the titration method. PA-doped membranes were soaked in 2 M sodium chloride solutions for 24 h at RT to ensure replacement of H^+ groups with Na^+ groups. Subsequently, the solution was titrated with 0.1 M sodium hydroxide.

Preparation of nanocomposite membranes

The PBI nanocomposite membranes were prepared by a solution-casting method using DMAc as a casting solvent. First, an appropriate amount of PBI powder was dissolved in DMAc under stirring at 120 °C. Then, different weight percentages of nanoparticles (2, 4, 8, 16 %) were dispersed in this solution using an ultrasonic bath. The obtained brown solution was cast onto a glass plate and solvent was removed by drying at 120 °C for 5 h. The membrane was removed from the glass plate by immersing in de-ionized water and the prepared membranes were immersed in PA. PBI-Fe_2TiO_5 nanocomposite membranes were named PFT. The thickness of PFT before doping PA was around 64–67 μm.

PFT_x were named for x wt% of Fe_2TiO_5 nanoparticles in the nanocomposite membranes.

Water uptake measurements of nanoparticles

A certain amount of nanoparticles was put into a test tube in 100 % RH for 24 h which was followed by weighing. After this procedure, Fe_2TiO_5 nanoparticles were dried for 24 h at 80 °C, followed by another weighing. Water uptake was determined by the difference between the weights of dry and fully hydrated nanoparticles. The water uptake of the nanoparticles was calculated by the following Eq. (1).

$$\mathrm{WU} = \frac{W_{\mathrm{NP/wet}} - W_{\mathrm{NP/dry}}}{W_{\mathrm{NP/dry}}} \times 100 \quad (1)$$

Where, $W_{\mathrm{NP/wet}}$ and $W_{\mathrm{NP/dry}}$ are weights of the wet and dry nanoparticles, respectively. The same procedure was repeated several times to ensure that the results are real.

Acid uptake of PFT_x membranes and leaching test of PA-doped PFT_x membranes

The PBI nanocomposite membranes were doped by immersion in aqueous PA (75 wt%) for 5 days. The membrane PA-doping contents were determined by weighing the membranes before and after doping of PA. In order to separate the water content from the PA doping before weighting, the membranes were dried by evaporating the water at 110 °C until the membranes' weight did not change with time.

The PA-doped PFT_x nanocomposite membranes were immersed in de-ionized hot water at 90 °C for 2 h. Then, the remaining acid was gained by a similar method as described above. Leaching test is a method for determining PA retained by the PA-doped PFT_x nanocomposite membranes, which is considered one of the main degradation factors of this sort of membranes in the fuel cell after washing with hot water.

FT-IR ATR spectra

The FT-IR ATR spectra were recorded in the range 600–4000 cm^{-1} using a Bruker Equinox 55 (attenuated total reflectance) operated at a resolution of 4 cm^{-1}.

Proton conductivity measurements

The impedance spectra were obtained by employing an AC impedance spectroscopy with PGSTAT303N potentiostat/galvanostat (Ecochemie). The sample membrane was immersed in aqueous PA (75 wt%) for 5 days at RT and then sealed between two platinum plates electrodes. The measurements were carried out on the potentiostatic mode. The frequencies were swept from 100 to 1 MHz recording 100 points with signal amplitude of 50 mV. The proton conductivty (σ) was calculated from the measured current resistance (R) using the equation ($\sigma = L/RA$), where, σ, L, R, A, respectively, refer to proton conductivity (S/cm), thickness (cm), resistance from the impedance data (Ω), and cross-sectional area (cm^2) of the membranes.

SEM, EDX, and mechanical properties measurements

The morphology of membranes was studied using a scanning electron microscope (SEM) (JSM-5600, Jeol Co.), coupled with energy dispersive X-ray (EDX) spectroscopy. The samples were freeze-fractured in liquid N_2 and then their surface was coated with gold plate before SEM observations were performed. The mechanical properties of the prepared membranes were measured by using Zwick/Roell Z030 tensile test machine. All the membranes were cut to the standard shape and all tests were performed at a crosshead speed of 10 mm/min and room temperature.

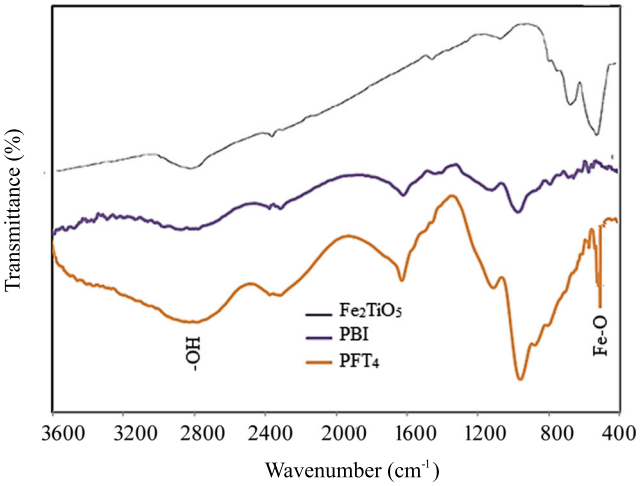

Fig. 1 FT-IR spectra of PBI and PFT_4 nanocomposite membranes and Fe_2TiO_5

Thermal properties

The thermal degradation behavior of the PA-doped nanocomposite membranes were measured using a thermogravimetric analysis (TGA) TA Instruments 2050 system, operated from 25 to 600 °C at the heating rate of 20 °C/min in nitrogen atmosphere.

XRD analysis

X-ray diffraction analysis (XRD) of PBI-based membranes was carried out on a rotating anode Philips PW-1700 diffractometer (l=1.5418 Å, Cu Ka).

Fuel cell tests

The catalyst was Pt–C (E-TEK, 20 wt% Pt) and the Pt loadings of anode and cathode were 0.5 mg/cm^2. Pt–C/PBI/LiCl/DMAc (3.6/1/0.2/38 by wt%) catalyst solution was prepared

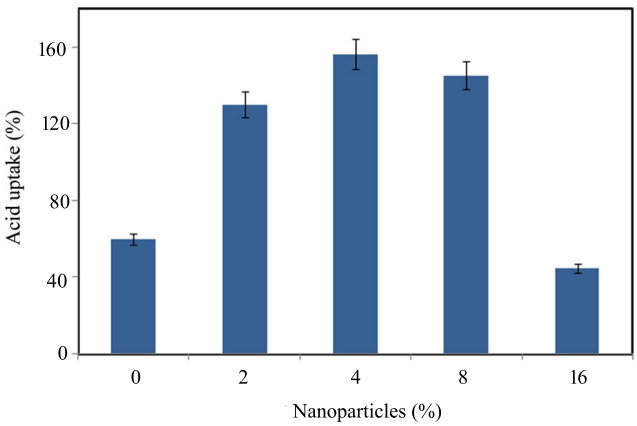

Fig. 2 Acid uptake plot of PFT_x nanocomposite membranes

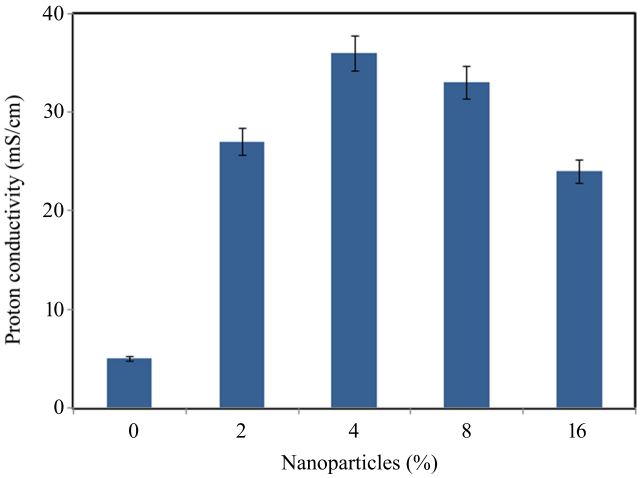

Fig. 3 Proton conductivity plots of PFT_x nanocomposite membranes at RT

by ultrasonic disturbing for 1 h. The Pt–C inks were loaded on to the carbon paper (Toray TGP-H-090) by a painting method and dried at 190 °C in a conventional oven to calculate catalyst loading. The catalyst coated carbon papers were then doped with PA by dipping in 10 % PA solution. The acid-doped membrane was sandwiched between two pieces of gas diffusion electrodes on each side and hot-pressed under a pressure of about 50 kg/cm^2 at 130 °C for 5 min.

Results and discussion

FT-IR ATR spectra

The results of the FT-IR spectra for PBI and PFT_4 nanocomposite and FT-IR spectra of neat-Fe_2TiO_5 are shown in Fig. 1. The PFT_4 nanocomposite membranes displayed numerous absorption peaks.

The characteristic absorption of PA molecules in PA-PBI membranes was investigated with FT-IR analysis. The bands at 500–1300 cm^{-1} refer to the vibration of HPO_4^{2-} and PA groups.

Three characteristic bands around 1090, 1008, and 970 cm^{-1} were respectively attributed to HPO_4^{2-}, P-OH, and $H_2PO_4^-$ stretching vibrations [9–11].

The bands at 1445 cm^{-1} suggest the deformation of benzimidazole "Breathing" mode of imidazole rings [25]. The peak at 1600 cm^{-1} was assigned to the C=C and C=N stretching groups. The absorption peaks at 2250–2500 cm^{-1} and 2500–300 cm^{-1} were owing to the stretching vibration of O–H and N^+–H in the presence of PA, respectively [26].

The peak at 2900 cm^{-1} corresponds to the stretching vibration of aromatic C–H groups. The bands at 3195 and 3390 cm^{-1} were attributed to the hydrogen bonded N–H groups and non-hydrogen bonded N–H stretching groups, respectively. The peak around 3615 cm^{-1} suggests the O–H stretching due to absorbed water [26].

Acid uptake and proton conductivity of PA-doped membranes

The acid uptake and proton conductivity of PA- PBI membranes were obtained at 60 % and 1.4 mS/cm, respectively. Figure 2 shows the acid uptake of PFT_x nanocomposite membranes. All of the PFT_x nanocomposite membranes confirmed a high acid uptake compared with pure PBI membranes. After acid doping with PA, the PA-PBI membranes exhibit enhancement of proton conductivity compared with the pure PBI membrane [7, 27–32]. The enhanced acid uptake of PFT_x nanocomposite membranes compared with PA-PBI membranes was attributed to the interaction of PA and Fe_2TiO_5 nanoparticles in PFT_x nanocomposite membranes. The added nanoparticles in the nanocomposite membranes enhanced the ability to trap PA, which improved the proton conductivity of the nanocomposite membranes (Fig. 3). Hence, PFT nanocomposite membranes displayed a high acid uptake and proton conductivity compared with PA-PBI membranes. In the PA-PBI nanocomposite membranes, protons can hop between the nitrogen of benzimidazole and PA by developing

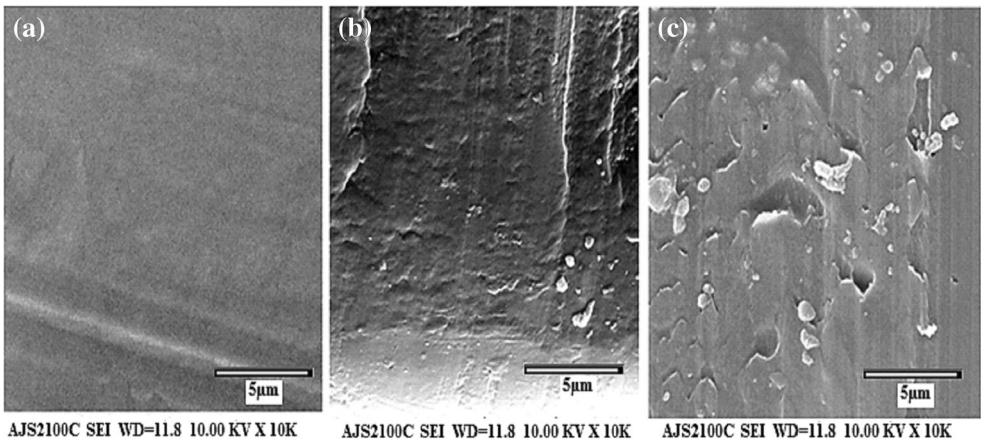

Fig. 4 SEM micrograph of the cross-section of (**a**) PFT_4, (**b**) PFT_{16} nanocomposite membranes

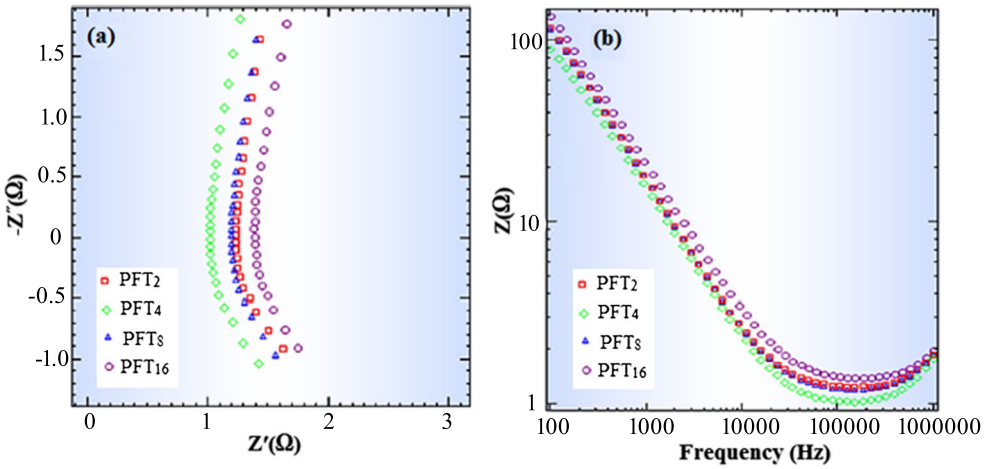

Fig. 5 Nyquist (**a**) and Bode modulus (**b**) plots for PFT_x nanocomposite membranes

benzimidazolium cation and dihydrogen phosphate anion, assisting proton conduction by a Grotthuss-type mechanism [30]. In this process, the proton hops between molecules (acid–acid, acid–water or acid–benzimidazole ring) in Grotthuss mechanism. The presence of HPO_4^{2-} and $H_2PO_4^-$ anions indicates that the proton transfer could occur according to the Grotthuss mechanism. In this mechanism, proton transfer between PA, HPO_4^{2-}, $H_2PO_4^-$, and PBI and strong acids could form membrane complexes due to the acid–base interaction or hydrogen bonding interactions between imidazole group of PBI membrane and acid molecules [30].

At high content of Fe_2TiO_5 nanoparticles (>4 wt%), there was a decrease in the acid uptake of PFT_x nanocomposite membranes. These results were attributed to the self-aggregate of Fe_2TiO_5 nanoparticles in PFT_x nanocomposite membranes. Figure 4 shows the SEM images of the cross-section of PBI, PFT_4, and PFT_{16} nanocomposite membranes. Figure 4a shows the SEM image of PBI and Fig. 4b shows that the PFT_4 nanocomposite membranes are homogenous. Significant agglomerations of Fe_2TiO_5 nanoparticles were clearly observable in the PFT_{16} nanocomposite membranes (Fig. 4c). This image shows that the aggregation of Fe_2TiO_5 nanoparticles happened at high content of Fe_2TiO_5 nanoparticles. The self-aggregate of nanoparticles reduces the active surface area of the nanoparticles and consequently the membrane acid uptake and proton conductivity were decreased.

Figure 5 demonstrated Nyquist and Bode modulus plots of PFT nanocomposite membranes (2–16 wt%) at fully hydrated state. Figure 5a shows that PFT_4 nanocomposite membranes displayed the lowest resistance (highest proton conductivity) compared with other PFT nanocomposite membranes. Bode modulus plots (Fig. 5b) approved a result obtained from Nyquist plots, which exhibited lower resistance for PFT_4 nanocomposite membrane corresponding to the Nyquist plots.

Water uptake measurement results of nanoparticles demonstrated that the Fe_2TiO_5 nanoparticles displayed a higher water uptake (10 %) compared with TiO_2 nanoparticles (3 %) for equal weights of the TiO_2 and Fe_2TiO_5 nanoparticles in 25 °C. This result shows that Fe_2TiO_5 nanoparticles have better hydrophilicity properties compared with TiO_2 nanoparticles. The proton conductivity of PFT_4 nanocomposite membranes has an intense increase compared with Nafion nanocomposite membrane [33–35] and other PBI-based nanocomposite membrane [36–41]. Table 1 shows a comparison between the proton conductivity of PFT_4 nanocomposite membranes and the other works. As it can be seen, the PFT_4 nanocomposite membranes show proton conductivity comparable to that of commercial Nafion membrane and significant increase in proton conductivity (78 mS/cm at 180 °C) in comparison with others. It seems that in Fe_2TiO_5 nanoparticles, once Fe^{3+} cations are located near Ti^{4+} cations, the acidic properties of these ions are increased. Therefore, PA ensures strong interaction with Fe_2TiO_5

Table 1 Specification of several of PA-doped PBI composite membranes

Inorganic phase	Filler content wt%	T (°C)	% RH/DC[a]	Proton conductivity (mS/cm)	Ref
Fe_2TiO_5	4	180	DC	78	This work
Silica	10	140	1	38	[36]
ZrO_2	10	180	DC	32	[37]
Zirconium phosphate	3	180	5	80	[38]
Silica	10	150	DC	67	[39]
Silica	10	160	DC	50	[40]
Sulfonated silica	10	160	DC	40	[41]

[a] Dry condition

nanoparticles in PA-doped nanocomposite membranes and as a result the proton conductivity of the PFT_4 nanocomposite membranes is developed because of the increasing capability of PA trap. To evaluate the proton conductivity of the PFT_x membranes in high temperature, the PFT_4 and the PFT_8 membranes which had much better proton conductivity than the PBI and other PFT_x membranes at RT were used for evaluation of proton conductivity in different temperatures up to 180 °C. Figure 6 shows the conductivity of PBI, PFT_4 and PFT_8 composite membranes at dry environment up to 180 °C. As it is seen in Fig. 6, these two membranes (PFT_4 and PFT_8) still exhibited higher proton conductivities than the pristine PA-PBI membrane. This finding could be due to the higher doping levels achieved in these membranes.

Leaching test of PA-doped PFT_x membranes

The acid leaching tests for PFT nanocomposite membranes were carried out in order to determine the PA preservation ability of the membranes. The acid leaching test is considered as one of the main degradation aspects of PBI-based membranes in the PEMFCs [42, 43]. Figure 7 displayed the results achieved from the leaching tests. The PFT_4 nanocomposite membranes preserve higher amounts of the PA than the other PFT_x nanocomposite membranes. This result shows that the presence of Fe_2TiO_5 in the PFT_4 nanocomposite membranes improved the capability properties of the membrane to retain acid after being washed with hot water. The formed agglomerates for PFT_{16} nanocomposite membranes increase the PA leaching from the membrane than the other PFT_x nanocomposite membranes.

Ion exchange capacity

The ion exchange capacity (IEC) of PFT_x nanocomposite membranes is displayed in Fig. 8. IEC values of PFT nanocomposite membranes increase with the increasing of the nanoparticles content due to higher PA trap of nanoparticles, which increased the dissociable H^+ ions. PFT_4 nanocomposite membranes displayed high IEC (meq g^{-1}) compared with other nanocomposite membranes. But in the high content of nanoparticles (>4 wt%) IEC values decreased due to the aggregation of nanoparticles.

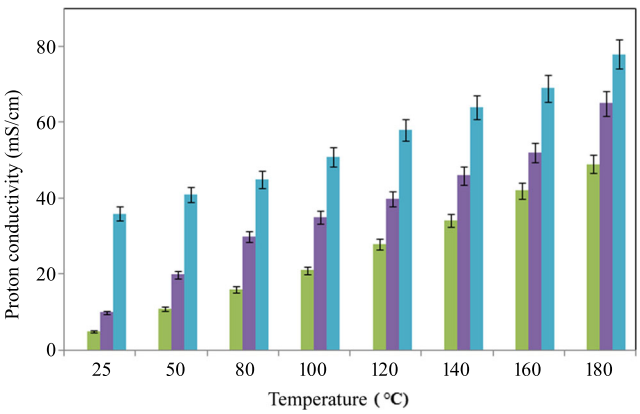

Fig. 6 Proton conductivity of PBI, PFT_4, and PFT_8 composite membranes at dry environment up to 180 °C

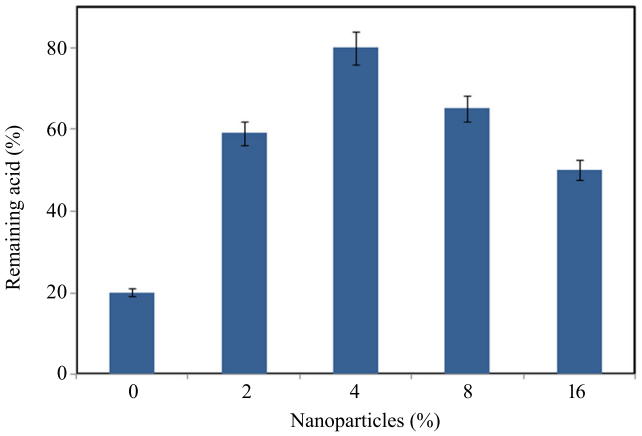

Fig. 7 Remaining acid plot of PFT_x nanocomposite membranes

EDX analysis and mechanical properties

EDX analysis established the presence of Fe_2TiO_5 in the PFT_4 nanocomposite membrane. EDX distribution of nanoparticles in the cross-section of PFT_4 nanocomposite membranes were demonstrated in Fig. 9a. A homogenous distribution of Fe and Ti nanoparticles in the cross-section of PFT_4 nanocomposite membranes were detected.

From Fig. 9b, it was found that the PFT_4 nanocomposite membranes, due to strong interactions of Fe_2TiO_5 nanoparticles with PBI-based membrane, displayed a higher mechanical stability than PBI-based membrane. Uniform dispersion of

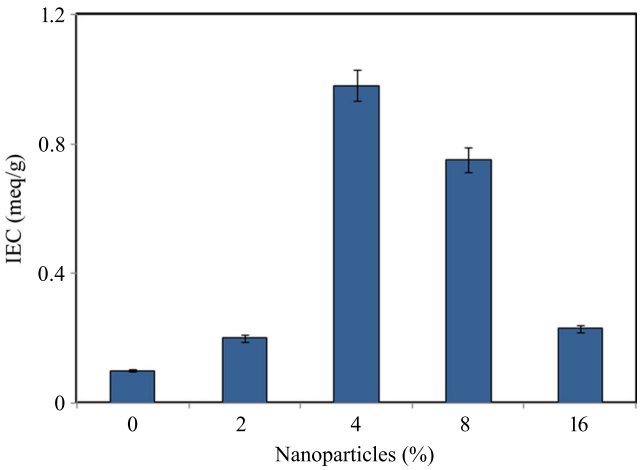

Fig. 8 Ion exchange capacity (IEC) of PFT_x nanocomposite membranes

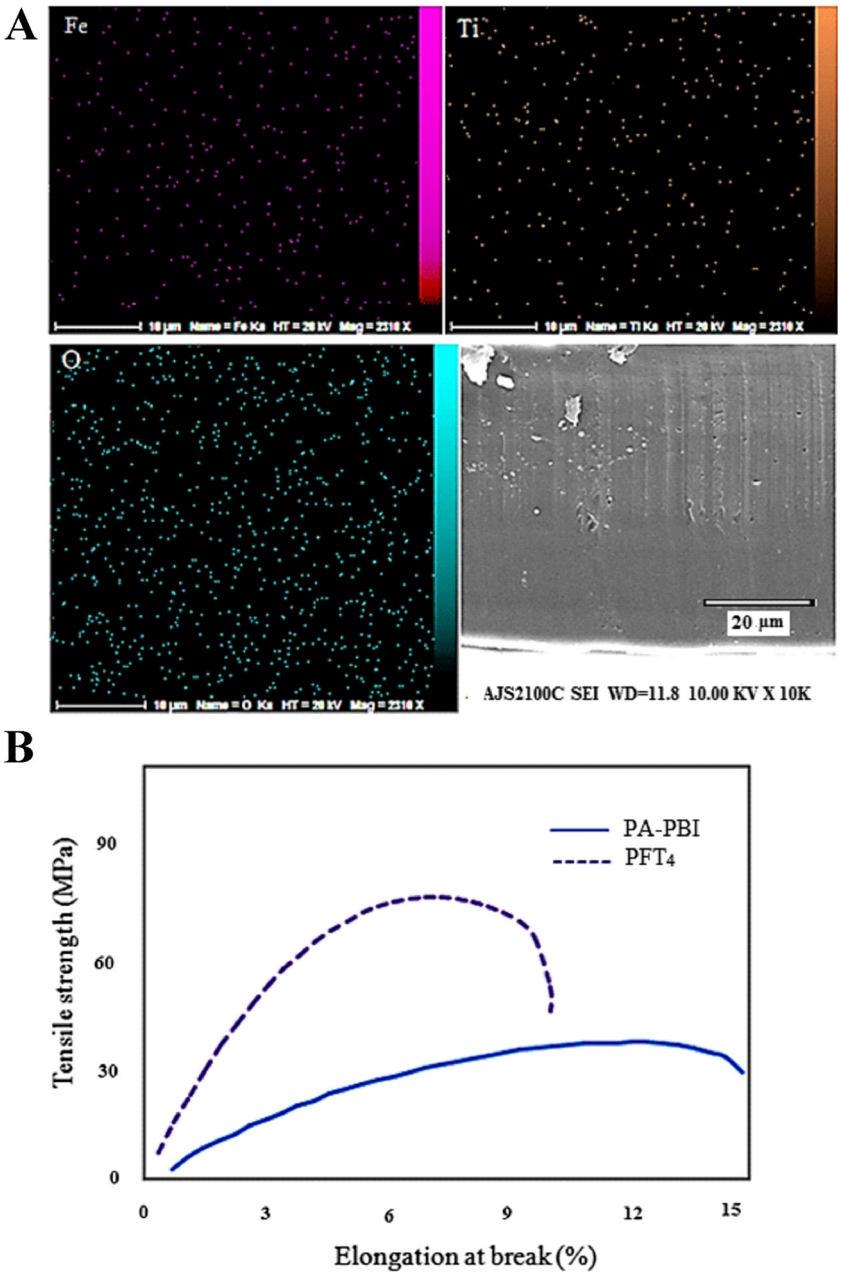

Fig. 9 SEM-EDX images of the cross-section of PFT_4 nanocomposite membranes (**a**) and mechanical stability plot of PA-PBI and PFT_4 membranes (**b**)

nanoparticles in the PFT_4 nanocomposite membranes, which increases the PBI-nanoparticles interactions, plays also a key role in improvement of its mechanical stability.

Thermogravimetric analyses

The results of the thermal stability for the PFT_x nanocomposite membranes are demonstrated in Fig. 10. From Fig. 10, it can be seen that the PFT_4 nanocomposites membranes displayed higher thermal stability than other nanocomposite membranes.

Incorporation of 4 wt% of Fe_2TiO_5 nanoparticles in PFT_4 nanocomposites membranes, which is an effective way for improving the thermal stability of nanocomposites membranes, leads to an increase in the decomposition temperature of PFT_4 nanocomposite membranes compared with other nanocomposite membranes.

Figure 10 shows that all the samples show two well-defined weight decays. The first goes from room temperature to 125 °C that is due to the desorption of absorbed water from polymer. And the second one, appearing at around 160 °C, is due to the thermal changes in PA, forming pyrophosphoric and triphosphoric acid, as shown by the following equations:

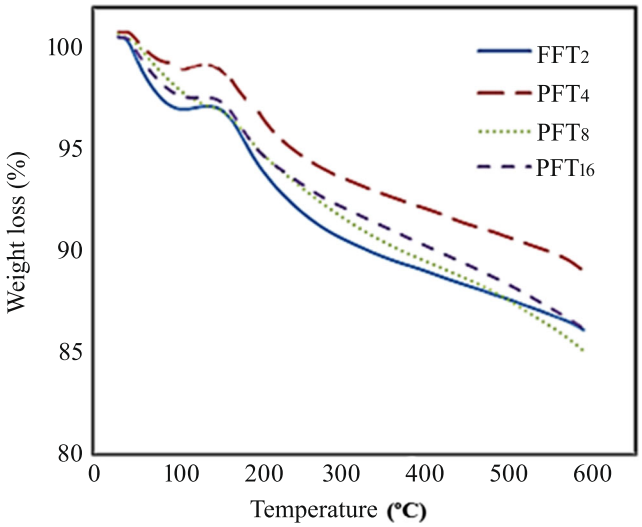

Fig. 10 Thermograms of the of PFT_x nanocomposite membranes

$$2H_3PO_4 \rightarrow H_4P_2O_7 + H_2O \quad (2)$$

$$3H_4P_2O_7 \rightarrow 2H_5P_3O_{10} + H_2O \quad (3)$$

The PFT_4 nanocomposite membranes show outstanding thermal stability. It also has displayed high proton conductivity and worked at high temperatures.

X-ray diffraction analyses PFT_x membranes

The X-ray patterns of the PFT nanocomposite membranes are shown in Fig. 11. The PFT nanocomposite membranes displayed a broad peak at around $2\theta=25°$. In Fig. 11, the Fe_2TiO_5 X-ray pattern is shown. All the PFT nanocomposite membranes displayed the main peak that is the characteristic of Fe_2TiO_5 nanoparticles. The more intense the main peak, the higher the content of Fe_2TiO_5 will be appear. This fact confirms the presence of the Fe_2TiO_5 nanoparticles in the PBI membranes and that the structure of it did not vary when incorporated into the membrane.

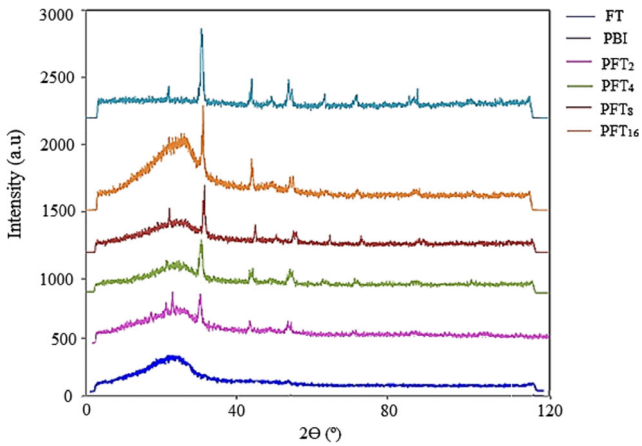

Fig. 11 X-ray diffraction patterns of the undoped standard PBI, PFT_x nanocomposite membranes, and Fe_2TiO_5 nanoparticles

Table 2 Fuel cell performance for unit cell based on PFT_4 nanocomposite membranes

T (°C)	OCV (V)	I (A/cm^2) in 0.5 V	PD (W/cm^2) in 0.5 V
100	0.84	0.40	0.20
150	0.84	0.51	0.26
180	0.86	0.76	0.38

Fuel cell performance tests

To evaluate the fuel cell performance of the PFT_x membranes, the PFT_4 membrane was used to prepare MEAs and the fuel cell performance test was carried out. The membrane thickness was around 65 μm. The PEMFC unit cell performance of these MEAs were tested at 100, 150, and 180 °C under ambient pressure with non-humidified H_2/O_2 flows. The flow rates for both hydrogen and oxygen gases were kept as 300 ml/min and 500 ml/min, respectively. Table 2 summarizes the PEMFC open circuit voltages (OCVs), power density in 0.5 V and the current density in 0.5 V. The PFT_4 composite membrane showed 380 mW/ cm^2 power density and 760 mA/cm^2 current density in 0.5 V at 180 °C at dry condition. Polarization curves were obtained using a fuel cell evaluation system (FCT—150 s). Figure 12 shows polarization curves for a fuel cell based on the PFT_4 nanocomposite membranes obtained at different temperatures (RT—180 °C) and PBI membranes obtained at 180 °C.

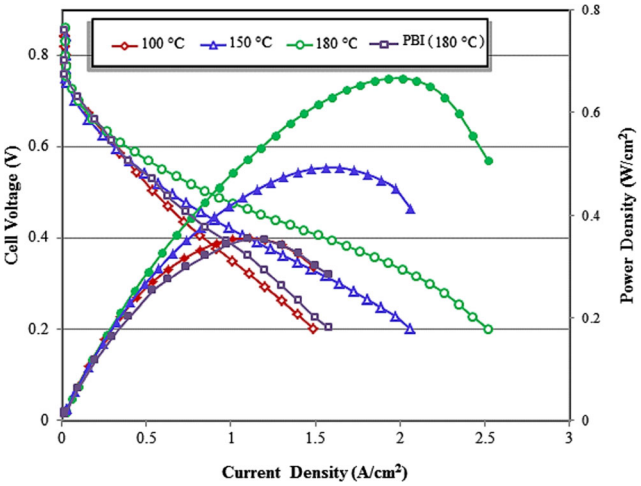

Fig. 12 Polarization curves for a fuel cell based on the PFT_4 nanocomposite membranes obtained at different temperatures (25–180 °C) and PBI membranes obtained at 180 °C

Conclusion

In the present study, new and advanced PBI-Fe_2TiO_5 nanocomposite membranes were prepared by solution-casting method. The results showed that the acid uptake and proton conductivity of the PFT nanocomposite membranes were higher than that of PBI-based membrane because of the unique properties of Fe_2TiO_5 nanoparticles. The PA-doped PFT_4 nanocomposite membrane showed a higher proton conductivity specially at high temperatures up to 180 °C (78 mS/cm) compared with the PA-doped PBI and showed 380 mW/cm^2 power density and 760 mA/cm^2 current density in 0.5 V and 180 °C at dry condition. These results indicated that the PBI nanocomposite membranes based on Fe_2TiO_5 could be utilized as good candidates as proton exchange membranes for high-temperature PEMFCs.

Acknowledgments The authors are grateful to the Renewable Energy Research Center (RERC), Amirkabir University of Technology (Tehran, Iran) for the financial support of this work.

References

1. Andujar JM, Segura F (2009) Fuel cells: history and updating. A walk along two centuries. Renew Sust Energ Rev 13:2309–2322
2. Tang H, Peikang S, Jiang SP, Wang F, Pan M (2007) A degradation study of Nafion proton exchange membrane of PEM fuel cells. J Power Sources 170:85–92
3. Chen CY, Garnica JI, Duke MC, Dalla RF, Dicks AL, Diniz JC (2007) Nafion/polyaniline/silica composite membranes for direct methanol fuel cell application. J Power Sources 166:324–330
4. He R, Li Q, Xiao G, Bjerrum NJ (2003) Proton conductivity of phosphoric acid doped polybenzimidazole and its components with inorganic proton conductors. J Membr Sci 226:169–184
5. Yang C, Srinivasan S, Bocarsly AB, Tulyani S, Benziger JB (2004) A comparison of physical properties and fuel cell performance of Nafion and zirconium phosphate/Nafion composite membranes. J Membr Sci 237:145–161
6. Lobato J, Canizares P, Rodrigo MA, Javier Pinar DUF (2011) A novel titanium PBI-based composite membrane for high temperature PEMFCs. J Membr Sci 369:105–111
7. Ma YL, Wainright JS, Litt MH, Savinell RF (2004) Conductivity of PBI membranes for high temperature polymer electrolyte fuel cells. J Electrochem Soc 151:8–16
8. Iwahara H, Esaka T, Uchida H, Maeda N (1981) Proton conduction in sintered oxides and its application to steam electrolysis for hydrogen production. Solid State Ionics 3(4):359–363
9. Tanaka R, Yamamoto H, Kawamura S, Iwase T (1995) Proton conducting behavior of poly(ethylenimine)-H_3PO_4 systems. Electrochim Acta 40:2421–2424
10. Wieczorek W, Stevens JR (1996) Proton transport in polyacrylamide based hydrogels doped with H_3PO_4 or H_2SO_4. Polymer 38:2057–2065
11. Higuchi T, Tsukamoto T, Sata N, Ishigame M, Kobayashi K, Yamaguchi S, Shin S (2002) Electronic structures of protonic conductors $SrTiO_3$ and $SrCeO_3$ by O 1s X-ray absorption spectroscopy. Solid State Ionics 154–5:735–739
12. Jones D J, Roziere J (2003) Inorganic/organic composite membranes. Handbook of fuel cells, Wiley 3:447–463
13. Ogoshi T, Chujo Y (2005) Organic–inorganic polymer hybrids prepared by the sol–gel method. Compos Interfaces 11:539–566
14. Christian P, Kammer F, Baalousha M, Hofmann T (2008) Nanoparticles: structure, properties, preparation and behaviour in environmental media. Ecotoxicology 17:326–343
15. Kozuka H, Kajimura M (2001) Sol–gel preparation and photo electrochemical properties of Fe_2TiO_5 thin films. J Sol-Gel Sci Technol 22:125–132
16. Tholence JL, Yeshurun Y, Wanklyn B (1986) Low-temperature study of the susceptibility in the anisotropic spin glass Fe_2TiO_5. Solid State Phys 19:235–239
17. Yu R, Li Z, Wang D, Lai X, Xing C, Yang M, Xing X (2010) Fe_2TiO_5/α-Fe_2O_3 nanocomposite hollow spheres with enhanced gas-sensing properties. Scripta Mater 63:155–158
18. Guanzhou Q, Jiang T, Hongxu L, Dianzuo W (2003) Functions and molecular structure of organic binders for iron ore pelletization. Colloids Surf A 224:11–22
19. Sun L, Wang S, Jin W, Hou H, Jiang L, Sun G (2010) Nano-sized Fe_2O_3-SO_4^{2-} solid superacid composite Nafion membranes for direct methanol fuel cells. Int J Hydrogen Energy 35:12461–12468
20. Mohammadi G, Jahanshahi M, Rahimpour A (2013) Fabrication and evaluation of Nafion nanocomposite membrane based on ZrO_2-TiO_2 binary nanoparticles as fuel cell MEA. Int J Hydrogen Energy 38:9387–9394
21. Beydaghi H, Javanbakht M, SalarAmoli H, Badiei A, Khaniani Y, Ganjali MR, Norouzi P, Abdouss M (2011) Synthesis and characterization of new proton conducting hybrid membranes for PEM fuel cells based on poly(vinyl alcohol) and nanoporous silica containing phenyl sulfonic acid. Int J Hydrogen Energy 133:10–16
22. Salarizadeh P, Javanbakht M, Abdollahi M, Naji L (2013) Preparation, characterization and properties of proton exchange nanocomposite membranes based on poly(vinylalcohol) and poly(sulfonicacid)-grafted silica nanoparticles. Int J Hydrogen Energy 38:5473–5479
23. Hooshyari K, Javanbakht M, Naji L, Enhessari M (2014) Nanocomposite proton exchange membranes based on Nafion containing Fe_2TiO_5 nanoparticles in water and alcohol environments for PEMFC. J Membr Sci 454:74–81
24. Enhessari M, Kargar Razi M, Etemad L, Parviz A, Sakhae M (2014) Structural, optical, and magnetic properties of the Fe_2TiO_5 nanoparticles. J Exp Nanosci 9:167–176
25. Kim SK, Kim TH, Jung JW, Lee JC (2009) Polybenzimidazole containing benzimidazole side groups for high-temperature fuel cell applications. Polymer 50:3495–3502
26. Lobato J, Canizares P, Rodrigo MA, Linares J (2006) Synthesis and characterisation of poly[2,2-(m-phenylene)-5,5-bibenzimidazole] as polymer electrolyte membrane for high temperature PEMFCs. J Membr Sci 280:351–362
27. Xing B, Savadogo O (1999) The effect of acid doping on the conductivity of polybenzimidazole (PBI). J New Mater Electrochem Syst 2:95–101
28. Savinell RF, Yeager E, Tryk D, Landau U, Wainright J, Weng D, Lux K, Litt M, Rogers C (1994) A polymer electrolyte for operation at temperatures up to 200°C. J Electrochem Soc 141:46–48
29. Bouchet R, Siebert E (1999) Proton conduction in acid doped polybenzimidazole. Solid State Ionics 118:287–299
30. Kawahara M, Morita J, Rikukawa M, Ogata KN (2000) Synthesis and proton conductivity of thermally stable polymer electrolyte: poly(benzimidazole) complexes with strong acid molecules. Electrochim Acta 45:1395–1398
31. Xiao L, Zhang H, Scanlon E, Ramanathan LS, Choe EW, Rogers D, Apple T, Benicewicz BC (2005) High-temperature polybenzimidazole fuel cell membranes via a sol–gel process. Chem Mater 17:5328–5333
32. Zhi-Gang S, Hongfeng X, Mingqiang L, Ming Hsing H (2006) Hybrid Nafion–inorganic oxides membrane doped with

heteropolyacids for high temperature operation of proton exchange membrane fuel cell. Solid State Ionics 177:779–785
33. Wu TZ, Sun G, Jin W, Hou H, Wang S, Xin Q (2008) Nafion and nano-size TiO_2–SO_4^{2-} solid superacid composite membrane for direct methanol fuel cell. J Membr Sci 313:336–343
34. Hammami R, Ahamed Z, Charradi K, Beji Z, Ben Assaker I, Auvity B, Squadrito G, Chtourou R (2013) Elaboration and characterization of hybrid polymer electrolytes Nafion-TiO_2 for PEMFCs. Int J Hydrogen Energy 38:11583–11590
35. Linlin M, Kumar Mishra A, Hoon Kim N, Hee Lee J (2012) Poly (2, 5-benzimidazole)–silica nanocomposite membranes for high temperature proton exchange membrane fuel cell. J Membr Sci 411:91–98
36. Zheng H, Mathe M (2011) Enhanced conductivity and stability of composite membranes based on poly (2,5-benzimidazole) and zirconium oxide nanoparticles for fuel cells. J Power Sources 196:894–898
37. Qian W, Shang Y, Fang M, Wang S, Xie X, Wang J, Wang W, Du J, Wang Y, Mao Z (2012) Sulfonated polybenzimidazole/zirconium phosphate composite membranes for high temperature applications. Int J Hydrogen Energy 37:12919–12924
38. Kumar Mishra A, Hoon Kim N, Hee Lee J (2014) Effects of ionic liquid-functionalized mesoporous silica on the proton conductivity of acid-doped poly(2,5-benzimidazole) composite membranes for high-temperature fuel cells. J Membr Sci 449:136–145
39. Suryani, Chang Y, Lai J, Liu Y (2012) Polybenzimidazole (PBI)-functionalized silica nanoparticles modified PBI nanocomposite membranes for proton exchange membranes fuel cells. J Membr Sci 403:1–7
40. Liu Y (2009) Preparation and properties of nanocomposite membranes of polybenzimidazole/sulfonated silica nanoparticles for proton exchange membranes. J Membr Sci 332:121–128
41. Devanathan R (2008) Recent developments in proton exchange membranes for fuel cells. Energy Environ Sci 1:101–119
42. Borup R, Meyers J, Pivovar B, Kim YS, Mukundan R, Garland N, Myers D, Wilson M, Garzon F, Wood D, Zelenay P, More K, Stroh K, Zawodzinski T, Boncella J, McGrath JE, Inaba M, Miyatake K, Hori M, Ota K, Ogumi Z, Miyata S, Nishikata A, Siroma Z, Uchimoto Y, Yasuda K, Kimijima K, Iwashita N (2007) Scientific aspects of polymer electrolyte fuel cell durability and degradation. Chem Rev 107: 3904–3951
43. Antonio Asensio J, Sanchez EM, Gómez-Romero P (2010) Proton-conducting membranes based on benzimidazole polymers for high-temperature PEM fuel cells. A chemical quest. Chem Soc Rev 39: 3210–3239